

LASERS. ACTIVE MEDIA

DOI: 10.1070/QEL16206

Eye-safe picosecond Raman laser

I.A. Gorbunov, O.V. Kulagin, A.M. Sergeev

Abstract. **The results of development of a picosecond Nd:YAG laser with SBS and SRS pulse compression are presented. The laser emits single-frequency radiation (one longitudinal cavity mode of a passively *Q*-switched master oscillator) with a pulse energy of 50 mJ at a pulse duration of about 30 ps and a pulse repetition rate of 100 Hz. The output laser wavelength is 1530 nm. The laser beam quality is close to the diffraction limit ($M^2 \leqslant 1.2$). Thermally induced phase distortions introduced into the laser beam by the active elements of laser amplifiers are studied and a method of their compensation is proposed. Using this method, we have developed, fabricated, and successfully tested aspherical optical elements compensating for thermal aberrations of active elements, which has allowed us to decrease the beam divergence and increase the output energy.**

Keywords: *Raman laser, pulse compression, eye-safe optical range.*

1. Introduction

Short-pulse lasers operating in the eye-safe spectral range 1.4–1.6 μm find application in many fields, including remote diagnostics, range finding, and materials treatment. Radiation in this spectral range is needed, in particular, to ensure safety in long open measurement channels.

One of the laser media generating eye-safe radiation is erbium (or erbium–ytterbium) glass emitting at a wavelength of 1.54 μm [1, 2]. However, the high thermal load at the low thermal conductivity of the material, as well as a small laser transition cross section, makes it difficult to use this glass for designing lasers with a high pulse repetition rate and a short pulse duration.

Some of these restrictions can be avoided by using erbium-doped yttrium aluminium garnet (Er:YAG). This garnet is pumped by an erbium glass laser or recently available laser diodes (LDs) emitting at a wavelength of 1470 or 1533 nm [3–5]. Nevertheless, some restrictions imposed by up-conversion processes and small emission cross sections at laser wavelengths of 1617 and 1645 nm make it difficult to obtain short pulses.

Another approach is based on the use of Nd:YAG or Nd:YVO_4 lasers with intracavity parametric conversion of their wavelengths [6–8]. However, the minimal pulse duration achieved by this method is ~1 ns. The main drawback of this approach is the necessity of parametric amplification of picosecond pulses, which leads to a low conversion efficiency.

In this work, we obtain eye-safe radiation using SRS conversion [9–12]. We used a 1319-nm Nd:YAG laser with frequency conversion in barium nitrate crystals [$Ba(NO_3)_2$] [10]. Previously, SRS conversion was used separately from SRS compression. In the present work, we use SRS compression of nanosecond pulses to picosecond at a relatively high repetition rate (see [13] and references therein) simultaneously with frequency conversion.

SRS compression of pulses was observed even in early studies on nonlinear optics [14]. Later, it was demonstrated that the use of SBS makes it possible to compress pulses in multipass amplifiers [15]. In the 1980s, it was shown that, combining SBS and SRS compression, it is possible to efficiently convert nanosecond pulses into picosecond ones [16]. Single-cascade SRS [17] and SBS [18] compression was also realised in counterpropagating beams, but this approach did not solve the problem of achieving high energy efficiency and power scaling.

2. Scheme of a picosecond Raman laser

The aim of the present work was to design an eye-safe laser emitting picosecond pulses with an energy up to 50 mJ and a repetition rate of 100 Hz. We used a scheme with a diode-pumped master oscillator (MO) and a lamp-pumped power amplifier. The diode-end-pumped master oscillator with a *Q*-switch made of vanadium-doped yttrium aluminium garnet (V:YAG) formed a single-longitudinal-mode 1319-nm beam with a pulse energy of 0.8 mJ, a pulse duration of 3.5 ns, and a divergence close to the diffraction limit.

Figure 1 shows the MO scheme. A beam with a wavelength of 808 nm propagates from a JOLD120-QPXF-2P pump laser diode (Jenoptik, Germany) through an optical fibre with a diameter of 600 μm and a numerical aperture of

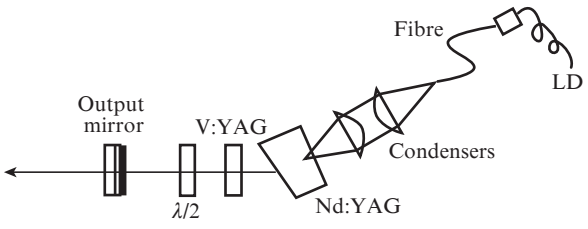

Figure 1. Scheme of a 1319-nm master oscillator.

I.A. Gorbunov, O.V. Kulagin, A.M. Sergeev Institute of Applied Physics, Russian Academy of Sciences, ul. Ul'yanova 46, 603950 Nizhnii Novgorod, Russia; e-mail: igorbunov@appl.sci-nnov.ru, ok@appl.sci-nnov.ru, ams@ufp.appl.sci-nnov.ru

Received 14 September 2016
Kvantovaya Elektronika **46** (10) 863–869 (2016)
Translated by M.N. Basieva

0.22 and is focused into a Nd:YAG active element (AE) by aspherical condenser lenses. The entrance face of the AE serves as a dichroic mirror, which has a high transmittance at wavelengths of 0.8 and 1.06 μm and a high reflectance at 1.32 μm. The other face of the AE is cut at the Brewster angle for a wavelength of 1.32 μm. This leads to suppression of oscillation at 1.06 μm due to the angular mismatch caused by the dispersion of the AE material. The MO cavity scheme also includes a V:YAG passive *Q*-switch and a crystalline quartz phase plate, which ensures selection (i.e., minimal losses) for only one of the Nd:YAG laser lines near 1.3 μm, namely, a line at 1.3188 μm. The total cavity length is about 3 cm.

The reflection coefficient of the output mirror is 62%. The Nd:YAG AE temperature is kept constant using a Peltier element, which removes heat to a water-cooled heat sink. The output MO pulses have a duration of 3.5 ns and an energy of 0.8 mJ at a repetition rate of 100 Hz. The pulse duration was measured by a Tektronix 3052B oscilloscope (transmission band 500 MHz) and a DFDMSh40–16 (NPF 'Dilaz') pin-photodetector with a transmission band of 16 GHz.

Then, laser pulses are fed to a four-pass amplifier, which includes three lamp-pumped laser heads (A1–A3) with Nd:YAG AEs 8 and 6.35 mm in diameter (Fig. 2). Each laser head contains two xenon pump lamps, whose radiation is reflected to the AEs by elliptical reflectors with a metal mirror coating. Faraday isolator 1 in the amplifier scheme consists of a polariser, a half-wave plate, and a Faraday rotator and does not allow the reflected radiation to return to the MO. A telescope forms a collimated beam of a required diameter (approximately 5.5 mm) from the initial diverging beam (hereinafter, the beam diameter is determined by a method of GOST R ISO 11146-1-2008 and, for Gaussian beams, is measured at e^{-2} of maximum intensity).

The horizontally polarised beam propagates through polarisers P1 and P2 and Faraday isolator 2, which consists of a Faraday rotator and a half-wave phase plate, and then through amplifiers A3 and A2, between which we placed a telescope repeater and a 90° quartz rotator. This scheme ensures compensation of thermally induced one-pass depolarisation in amplifiers A3 and A2 [19]. As a result of action of thermal lenses induced in A2 and A3, the laser beam becomes convergent. The lenses placed between A2 and A1 adjust the beam size to the aperture of the A1 amplifier and make the beam divergent so that it became collimated at the exit from A1 due to the thermal lens induced in A1. A dichroic mirror with a high transmittance at a wavelength of 1.32 μm and a high reflectance at 1.06 μm is placed between A2 and A1. This mirror is inclined to avoid spurious oscillation at 1.06 μm in the amplifiers. The radiation polarisation plane rotates by 90° after a double pass through the Faraday rotator.

It is known that one cascade of nonlinear optical compression usually shortens pump pulses by 20–30 times [13, 20]. To achieve a picosecond duration of output laser pulses, we used SBS compression in the multipass amplifier after the first two passes, which shortened the amplified pulse duration to subnanosecond. For this purpose, the beam reflected from a highly reflecting mirror and passed backward through the same amplifiers (second pass) is reflected by polariser P2 due to the polarisation plane rotation. A lens focuses the radiation into an SBS cell, in which phase conjugation and SBS compression of the optical pulse occur. Phase conjugation compensates for the beam aberrations and distortions appear-

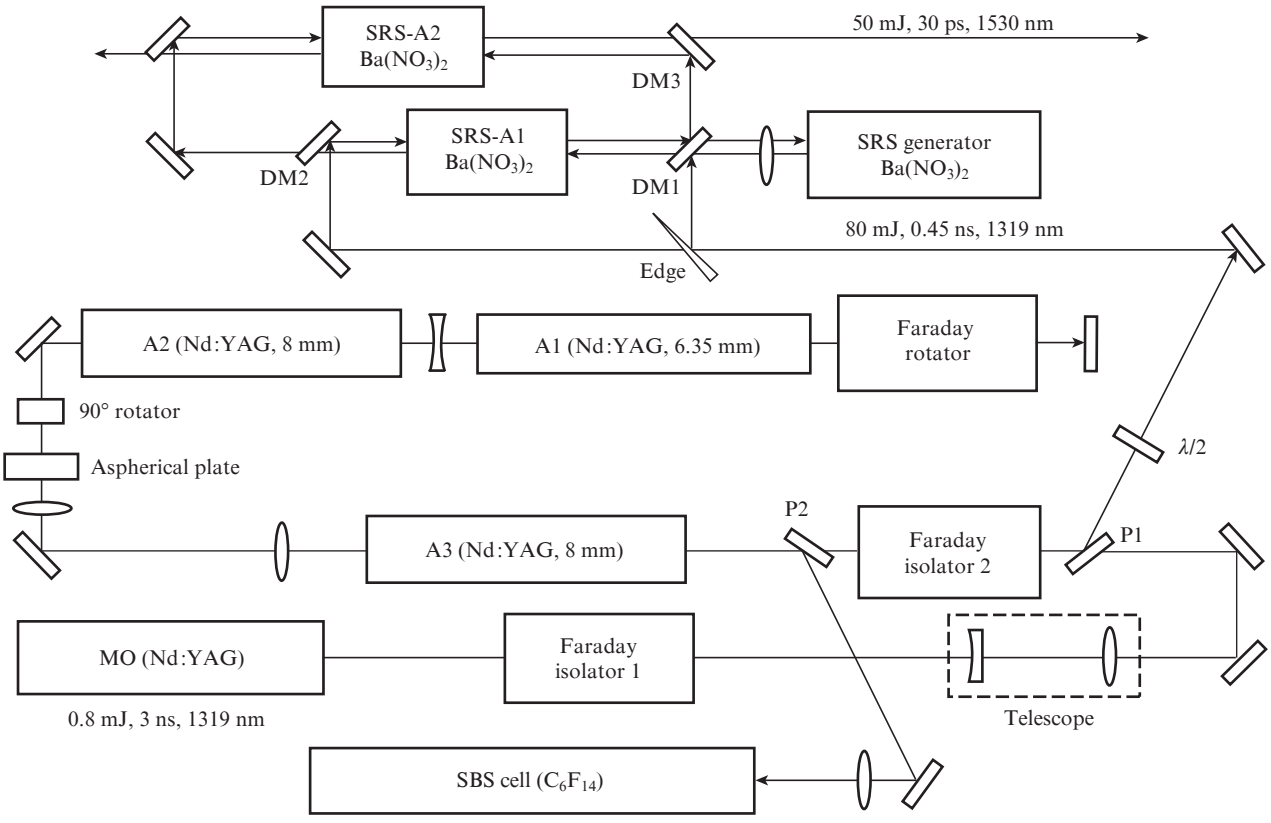

Figure 2. General scheme of a laser with SRS pulse compression.

ing as a result of propagation through amplifiers, while compression decreases the pulse duration to 0.3–0.5 ns (pulse duration was measured using an S7-19 fast oscilloscope with a transmission band of 5 GHz). The SBS compression was optimised by the method described in [20]. We used a stainless steel cell 50 cm long, which was filled with high-purity-grade perfluorohexane (C_6F_{14}). In the optimal geometry, a beam 4 mm in diameter at the entrance to the cell is focused by a lens with a focal length of +270 mm. In this case, the MO pulse with a duration of 3.5 ns was compressed to 0.45 ns (Fig. 3). The phase-conjugated beam makes the third and fourth passes thought the amplifiers and, after passing Faraday isolator 2, is coupled out by polariser P1 into a SRS compressor. After four amplification passes, the laser pulse energy is 80–90 mJ at a pulse duration of 0.45 ns.

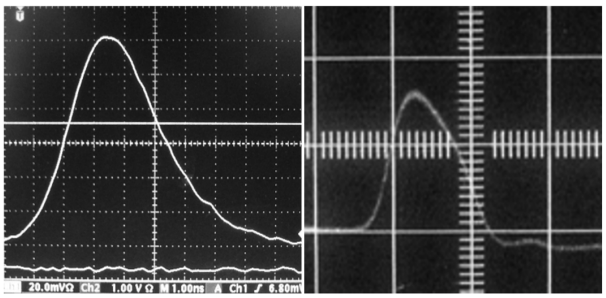

a b

Figure 3. (a) MO output pulse (sweep rate 1 ns div^{-1}) and (b) amplifier output pulse after SBS compression (sweep rate 0.5 ns div^{-1}).

The SRS compression scheme includes a SRS generator and two SRS amplifiers (SRS A1 and SRS A2) (Fig. 2). As a nonlinear medium for SRS conversion, we used barium nitrate crystals $Ba(NO_3)_2$ [21] with a relatively high (~ 8 cm GW^{-1}) local SRS gain increment at 1319 nm, a satisfactory Raman frequency shift (1047 cm^{-1}), and a high breakdown threshold. Dichroic mirrors DM1, DM2, and DM3 have high reflectance at 1.32 μm and high transmittance at the Stokes wavelength 1.53 μm. About 1% of the laser radiation is reflected by an edge and mirror DM1 to the SRS generator. The SRS generator geometry and the focusing lens were optimised to achieve efficient compression of Stokes pulses in the SRS process. The 1.53-μm radiation propagates back through DM1 and is amplified in SRS A1 as a result of interaction with counterpropagating 1.32-μm pump radiation. Additional lenses, which are not shown in the scheme, change the size and divergence of interacting beams and are selected to optimise Raman conversion in the amplifiers. The mirrors direct the Stokes and pump pulses so that they meet in SRS A2 again counterpropagating to each other.

It is known [13, 16] that the conditions needed to achieve efficient pulse compression are as follows: the Raman medium length must exceed half of the pulse length in the medium and the focal waist length must be approximately 25 times shorter than the distance from the medium entrance to the waist. Therefore, the crystals 70–80 mm long used in the laser are well suitable for SRS conversion of pulses of the given duration. To satisfy the second condition, we used a lens with a focal length of +100 mm to focus the beam into the SRS generator. As a result, the most part of the initial pump pulse energy with $\lambda = 1.32$ μm and a duration of about 0.45 ns was converted into a compressed Stokes pulse with a wavelength of 1.53 μm, a duration of 30–50 ps, and an energy up to 50 mJ. Part of the radiation power in the SRS process was spent to heat the barium nitrate crystals, but this caused no noticeable thermooptical effects and corresponding laser beam distortions. The laser beam quality was measured using an Ophir-Spiricon SP620U camera and found to be $M^2 \leqslant 1.2$ at the laser exit. The compressed pulse duration at half maximum estimated from the autocorrelation function (ACF) was ~30 ps (Fig. 4).

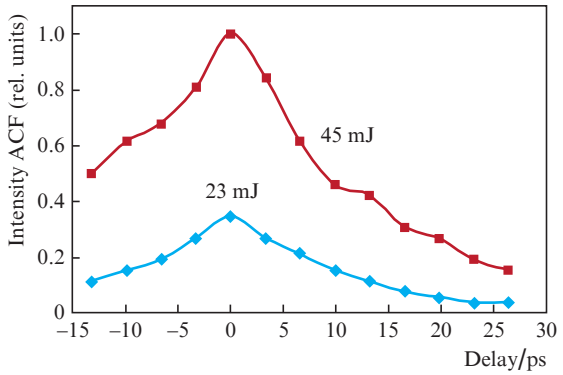

Figure 4. Autocorrelation function of a laser output pulse at a wavelength of 1530 nm (after an SRS compressor) at output energies of 23 and 45 mJ.

3. Compensation of thermally induced phase distortions of the amplified laser beam and improvement of its quality

One of the problems of creation of this laser is the existence of thermal effects in the AEs of amplifier heads, which is typical for lasers with high average powers. Thermal lens aberrations and thermally induced depolarisation in the four-pass amplifier were found to be significant; these effects were taken into account and minimised. In particular, the thermally induced depolarisation in the A2 and A3 amplifiers was compensated using a scheme with a telescope repeater and a 90° quartz rotator [19]. Compensation in A1 was achieved due to polarisation plane rotation by 90° after two passes of the beam through a Faraday rotator (see Fig. 2). Figure 5 shows the

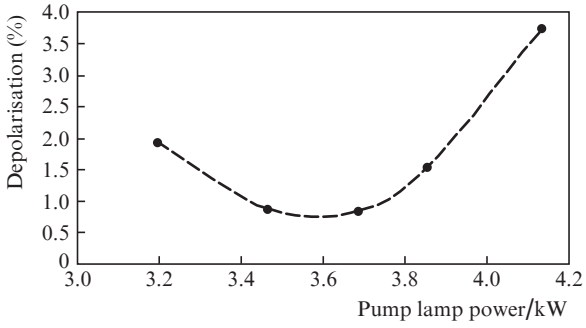

Figure 5. Amplified pulse depolarisation measured after propagation through A2 and A3 as a function of the power of A2 lamp pumping at the A3 pump power of 3540 W.

depolarisation degree of the amplified beam measured after propagation through A2 and A3 as a function of the A2 lamp pump power at a fixed (3450 W) A3 pump power.

We measured the power of thermal lenses induced in each of the amplifier heads as a function of the pump lamp power. The electric discharge energy in the lamps was determined by measuring the pulse current and voltage. Note that the pump lamp power supplies operated with discharge interruption (Fig. 6) to decrease the thermal load on the AEs, because the time of incidence of an amplified pulse on the AE usually corresponds to the time of the maximum gain, which is close to the time of the maximum discharge current and the rear part of the common bell-like discharge pulse is useless for laser pulse amplification but enhances the AE heating. The lamp current pulse for each light pulse was recorded by a Hall detector, the data of which were delivered to a computer via an AD converter with a sampling rate of 400 kHz, while the voltage at the pump lamps was controlled by their power supplies. These measurements allowed us to estimate the average electric pulse energy and its root-mean-square deviation in each lamp.

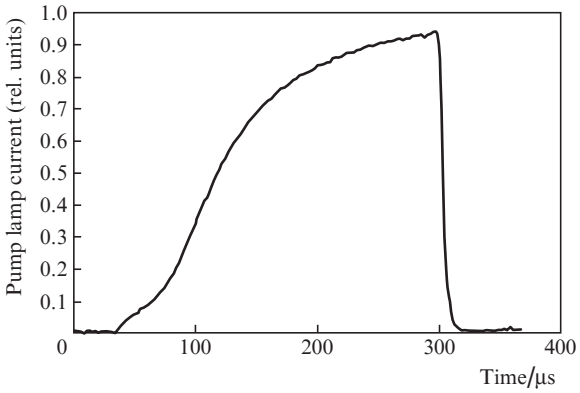

Figure 6. Discharge current pulse in pump lamps of amplifiers.

To measure the focal distance of a thermal lens, one should send a collimated beam from the MO to the amplifier and then to measure the distance from the beam focal waist to the plane corresponding to the main plane of the thermal lens [19]. Based on these measurements, we chose lenses for compensating the beam divergence needed to obtain a collimated beam at the exit from amplifier A1. Figure 7 shows the measured optical powers of the thermal lens as functions of the electric pump power in amplifiers with AEs 6.35 and 8 mm in diameter.

However, the compensation of thermal lenses only by spherical lenses turned out to be insufficient to retain a good beam quality. A beam with a diameter of 5.5 mm at the entrance was observed to be considerably narrower (to 1.85 mm) after four amplification passes. As a result, the high energy density in the beam centre led to breakdown in the output unit, i.e., in the Faraday isolator. In addition, the beam narrowing obviously decreases the amplification efficiency due to a poor filling of the AE aperture by the amplified radiation in the last amplification pass. The attempts to increase the beam diameter at the entrance did not lead to an increase in the beam diameter at the amplifier exit. Based on this, we made a conclusion (which was then confirmed by calculations) about

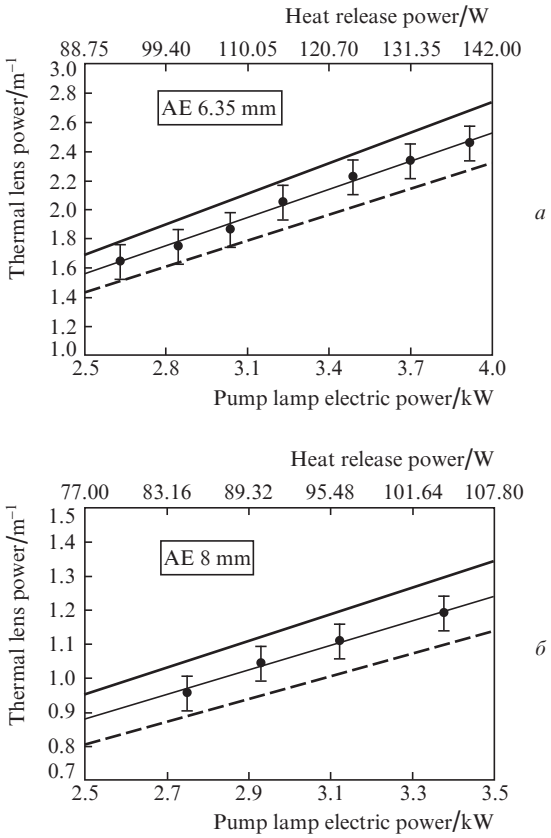

Figure 7. Dependences of the measured optical power of the thermal lens on the electric power of pump lamps (points) and corresponding calculated optical power for the radial (solid lines) and tangential (dashed lines) polarisation modes as functions of the heat release power in AEs with diameters of (a) 6.35 and (b) 8 mm.

existence of phase distortions in the amplifier AE that were not compensated for by spherical lenses.

To calculate thermal phase distortions, it is necessary first to find the temperature profile $T(r)$ in the AE from the thermal conductivity equation

$$\frac{1}{r}\frac{\partial}{\partial r}\left(K(T)r\frac{\partial T}{\partial r}\right) = -Q(r)\ , \qquad (1)$$

where $Q(r)$ is the heat release power density, i.e., the density of the part of pump power spent on heating of the AE, and $K(T)$ is the thermal conductivity of the AE material. In the classical calculation of thermal lenses in (111) oriented Nd:YAG rods [22], the $Q(r)$ and $K(T)$ dependences are not taken into account and assumed to be constant, as well as the parameter $\mathrm{d}n/\mathrm{d}T$. In this case, the temperature and refractive index profiles $T(r)$ and $n_{r,\varphi}(r)$ are parabolic, which corresponds to a thermal lens without aberrations for each of the two polarisation modes. When $Q(r)$, $K(T)$, and $(\mathrm{d}n/\mathrm{d}T)(T)$ are taken into account, the refractive index profile becomes more complex, i.e., it is necessary to consider additional terms in the expansion of $n(r)$ in powers of r^2.

The heat release profile was assumed to be parabolic. To estimate the inhomogeneity of the pump profile and, hence, of heat release $Q(r)$, we measured the small-signal gain in different AE regions at a wavelength of 1.32 μm (Fig. 8). In this case, the input laser pulse energy was kept sufficiently low to

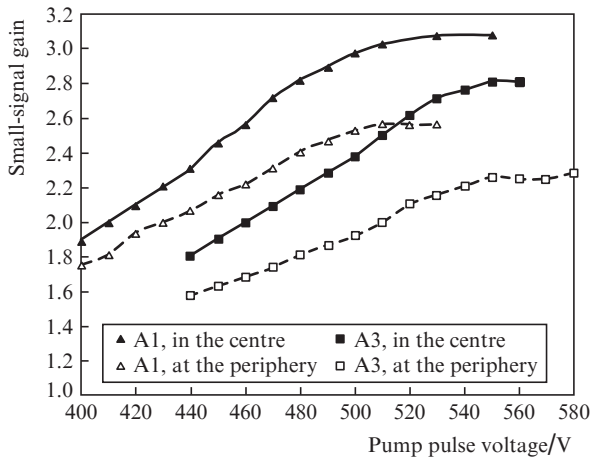

Figure 8. Small-signal gain at $\lambda = 1.32$ μm in the A3 and A1 amplifiers with AEs 8 and 6.35 mm in diameter, respectively, versus the pump lamp voltage.

avoid gain saturation in the AE. The amplified beam diameter was ~1 mm, i.e., was considerably smaller than the AE diameter, which allowed us to estimate the inhomogeneity of AE pumping by measuring the gain inhomogeneity over the AE cross section.

The found ratio between the gain coefficients in the centre and at the periphery of the AE corresponds to a decrease in the stored energy density from the centre to the periphery by 24% ± 2% and by 14% ± 2% for amplifiers with AEs 8 and 6.35 mm in diameter, respectively. Based on these measurements, we obtained the heat release profile

$$Q(r) = \frac{1}{1-0.5\beta}\frac{P}{\pi RL}\left[1-\beta\left(\frac{r}{R}\right)^2\right]. \quad (2)$$

Here, the measured β are 0.24 and 0.14 for AEs with diameters of 8 and 6.35 mm, respectively; P is the total heat release power; R is the AE radius; and L is the length of the pumped region of the AE. Then, to calculate the $T(r)$ profile, we used the $K(T)$ dependence [23]

$$K(T) = K_0\left(\frac{T_0}{T}\right)^{\zeta}, \quad (3)$$

where $\zeta = 0.7$, $T_0 = 300$ K, and $K_0 = 10.5$ W m^{-1} K^{-1}. In this case, the solution of Eq. (1) is

$$T(r) = T_p\exp\left\{1+\frac{P}{4\pi LT_pK(T_p)}\frac{1-\zeta}{1-0.5\beta}\times\left[1-\left(\frac{r}{R}\right)^2-\frac{\beta}{4}\left(1-\left(\frac{r}{R}\right)^4\right)\right]\right\}^{(1-\zeta)^{-1}}, \quad (4)$$

where $T_p = T(R)$ is taken to be 320 K. The refractive index profile is

$$n_{r,\varphi}(r) = n_0 + \Delta n_T(r) + \Delta n_{r,\varphi}(r). \quad (5)$$

Here, $n_0 = 1.82$ is the refractive index at 300 K and $\Delta n_T(r)$ and $\Delta n_{r,\varphi}(r)$ are the changes in n caused by temperature and photoelasticity effect, respectively. The term $\Delta n_T(r)$ was calculated using the temperature dependence of dn/dT

$$\frac{dn}{dT}(T) = \frac{dn}{dT_{300\,K}} + \frac{d^2n}{dT^2}(T-300\,K),$$

where $dn/dT_{300\,K} = 9.1\times10^{-6}$ K^{-1} and $d^2n/dT^2 = 3.8\times10^{-8}$ K^{-2} [23]. Then,

$$\Delta n_T(r) = \frac{dn}{dT_{300\,K}}(T(r)-300\,K) + \frac{1}{2}\frac{d^2n}{dT^2}(T(r)-300\,K)^2. \quad (6)$$

The refractive index variations $\Delta n(r)_{r,\varphi}$ appearing for two polarisation modes due to mechanical stresses in the AE and photoelasticity were calculated by the method described in [22]. We used for calculation the following Nd:YAG characteristics: Young's modulus $E = 280$ GPa, Poisson's ratio $\nu = 0.25$, thermal expansion coefficient $\alpha = 7.5\times10^{-6}$, and photoelasticity tensor components $p_{11} = -0.029$, $p_{12} = 0.0091$, $p_{44} = -0.0615$.

The changes in the refractive indices turn out to be different for the radial and tangential polarisation modes, but, due to the use of the scheme with two identical amplifiers and a 90° polarisation rotator, we can use the sum $\Delta n_{sum}(r) = \Delta n_r(r) + \Delta n_\varphi(r)$ to calculate the optical path in two amplifiers. To analyse the phase distortions in each amplifier, it is convenient to use the optical path difference for beams on and off the axis

$$OPD(r) = L[n(r) - n(0)]. \quad (7)$$

Here, we assume that the beams are straight and parallel to the AE axis. The obtained OPD(r) profile can be approximated by the parabola

$$OPD(r) \approx -\frac{D}{2}r^2, \quad (8)$$

where D is the optical power of the thermal lens. Comparison of the measured and calculated thermal lens powers allows us to find the relation between the electric power of pump lamps and the heat release power in the AE (Fig. 8) and use this relation in subsequent calculations. An interesting result is that the determined heat release is 3.55% and 3.08% of the total power of electric pump pulses for AEs with diameters of 6.35 and 8 mm, respectively. To take into account spherical aberrations, we approximate OPD(r) by the function

$$OPD(r) \approx -\frac{D'}{2}r^2 + C_4r^4, \quad (9)$$

where D' corresponds to the optical power of a parabolic lens and C_4 characterises spherical aberration. The dependences of calculated C_4 on the heat release power are shown in Fig. 9. The C_4 parameter is convenient to use to estimate the influence of aberrations on the beam quality. The M^2 parameter for a Gaussian beam passed through an element with spherical aberration can be found by the formulas [24]

$$M^2 = \left[1+(M_q^2)^2\right]^{1/2},\ M_q^2 = \frac{2\sqrt{2}\,\pi}{\lambda}C_4w^4, \quad (10)$$

where w in the Gaussian beam radius and λ is the wavelength.

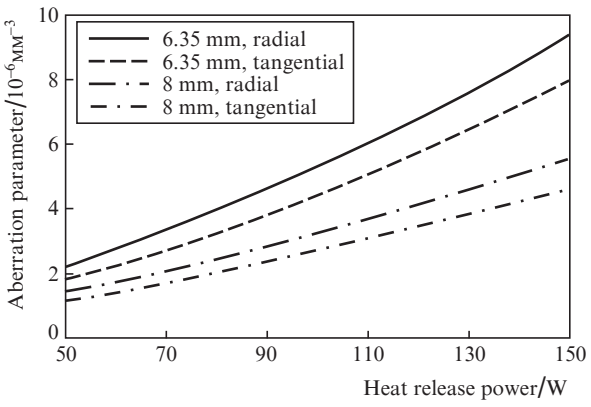

Figure 9. Dependences of calculated aberration parameters C_4 on the heat release power for radial and tangential polarisation modes in AEs with diameters of 6.35 and 8 mm.

To compensate for spherical aberrations, we used an aspherical K8 glass plate with the surface profile $z(r) = 8\times 10^{-6}\text{mm}^{-3}\cdot r^4$, which was produced on our request at the OAO NPO 'State Institute of Applied Optics'. One can see from (10) that the spherical aberration effect strongly depends on the laser beam diameter. The aspherical plate was placed between the telescope repeater and the A2 amplifier, where the beam is convergent and its diameter is larger than in each of the amplifiers. For correct compensation of aberrations, it was necessary to precisely choose the plate position with respect to A2. A scheme including one pass of the four-pass amplifier was modelled in the Zemax program, while the aspherical plate position was found as a result of optimisation in order to minimise the total spherical aberration of the optical system.

To check the efficiency of the aspherical aberration compensation, we measured the beam quality parameter M^2 after propagation through the A3 and A2 amplifiers with and without an aspherical plate. At a nominal pump power in each amplifier, which corresponds to a heat release of 110 W, the quality parameter M^2 was 2.9 ± 0.2 and 1.03 ± 0.1 without and with a plate, respectively (see Fig. 10). Thus, we achieved almost complete compensation of spherical aberration. At a measured beam diameter at the amplifier entrance of 5.45 ± 0.05 mm and $C_4 = 6.78\times10^{-6}$ mm^{-3} corresponding to propagation through amplifiers A3 and A2, calculation by (10) for a Gaussian incident beam yields $M^2 = 2.7\pm0.1$. This agrees well with the experimental result. Similar calculation for A1 taking into account beam scaling shows that the beam quality decreases only to $M^2 = 1.12$, which points to a much weaker aberration effect in this amplifier. As a result of aberration compensation, we managed to increase the beam diameter from 1.85 to 3.1 mm at the exit from the four-pass amplifier.

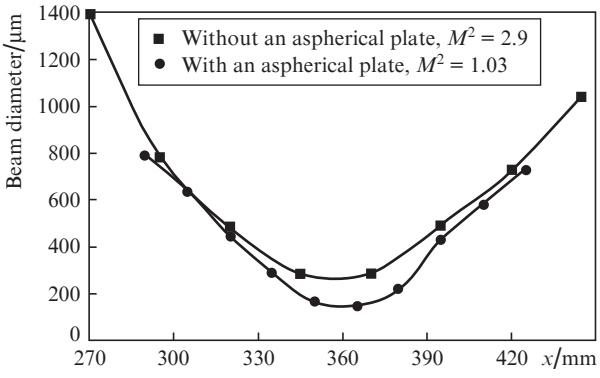

Figure 10. Beam diameter measured near the focal waist after amplifiers A3 and A2.

4. Conclusions

Thus, we have developed and tested a picosecond eye-safe Raman laser. Due to nonlinear optical pulse compression, we obtained an output pulse duration of 30 ps at a pulse energy of 50 mJ, a pulse repetition rate of 100 Hz, and a beam quality close to the diffraction limit ($M^2 \leqslant 1.2$). The combination of SRS and SBS compression ensures a more than hundred-fold pulse compression simultaneously with wavelength conversion into the eye-safe region due to Raman frequency shift. In the course of this work, we have studied thermal aberrations of a laser beam in amplifier rods caused by inhomogeneous pump distribution in the AE and by the temperature dependence of the physical parameters of yttrium aluminium garnet. A method of calculation of these thermal aberrations has been developed. As a result, a method of compensation of these aberrations has been proposed and used to develop, fabricate, and successfully test aspheric elements, namely, lenses with a surface profile corresponding to a quartic parabola, which compensate for thermal aberrations of active elements and thus allow one to achieve a diffraction-limited beam quality and increase the output pulse energy.

Acknowledgements. This work was partly supported by the Programme of Fundamental Research of the Physical Sciences Division of the Russian Academy of Sciences IV.2.5 'New nonlinear optical materials, structures, and methods for development of laser systems with unique characteristics'.

References

1. Häring R., Paschotta R., Fluck R., Gini E., Melchior H., Keller U. *J. Opt. Soc. Am. B*, **18**, 1805 (2001).
2. Setzler S.D., Francis M.P., Young Y.E., Konves J.R., Chicklis E.P. *IEEE J. Sel. Top. Quantum Electron.*, **11**, 645 (2005).
3. Kim J.W., Shen D.Y., Sahu J.K., Clarkson W.A. *IEEE J. Sel. Top. Quantum Electron.*, **15**, 361 (2009).
4. Chang N.W.H., Simakov N., Hosken D.J., Munch J., Ottaway D.J., Veitch P.J. *Opt. Express*, **18**, 13673 (2010).
5. Tang P., Zhou R., Zhao C., Xu C., Liu J., Zhang H., Shen D., Wen S. *Appl. Opt.*, **53**, 7773 (2014).
6. Mason P.D., Perrett B.J. *Advanced Solid State Photonics, OSA Technical Digest Series* (Washington: OSA, 2007) MB9.
7. Chen Y.F., Chen S.W., Tsai L.Y., Chen Y.C., Chien C.H. *Appl. Phys. B*, **79**, 823 (2004).
8. Chu H., Zhao J., Yang K., Zhao S., Li T., Li D., Li G., Qiao W. *Photon. Res.*, **3**, 260 (2015).
9. Tucker J.P., Oien A.L., Bennett G.T. *Proc. Conf. on Lasers and Electro-Optics* (Washington, DC: OSA, 2004) CMP1.
10. Murray J.T., Powell R.C., Peyghambarian N., Smith D., Austin W., Stolzenberger R.A. *Opt. Lett.*, **20**, 1017 (1995).
11. Basiev T.T., Doroshenko M.E., Osiko V.V., Sverchkov S.E., Galagan B.I. *Laser Phys. Lett.*, **2**, 237 (2005).
12. Dashkevich V.I., Shpak P.V., Voitikov S.V., Chulkov R.V., Grabtchikov A.S., Cheshev E.A., El-Desouki M., Orlovich V.A. *Opt. Commun.*, **351**, 1 (2015).
13. Pasmanik G.A., Shklovsky E.I., Shilov A.A., in *Phase Conjugate Laser Optics.* Ed. by A. Brignon and J.-P. Huignard (New York: John Wiley & Sons Inc., 2005) Ch. 7.
14. Maier M., Kaiser W., Giordmaine J.A. *Phys. Rev. Lett.*, **17**, 1275 (1966).

15. Hon D.T. *Opt. Lett.*, **5**, 516 (1980).
16. Buzyalis R.R., Girdauskas V., Dement'ev A.S., Ivanov V.B., Kosenko E.K., Mak A.A., Papernyi S.B., Serebryakov V.A. *Kvantovaya Elektron.*, **14**, 2266 (1987) [*Sov. J. Quantum Electron.*, **17**, 1444 (1987)].
17. Kulagin O.V., Kotov A.K., Pasmanik G.A. *Proc. Conf. Lasers and Electro-Optics* (Washington: OSA, 2004) CMP7.
18. Dement'ev A.S., Demin I., Murauskas E.K., Slavinskis N. *Kvantovaya Elektron.*, **41**, 153 (2011) [*Quantum Electron.*, **41**, 153 (2011)].
19. Lü Q., Kugler N., Weber H., Dong S., Müller N., Wittrock U. *Opt. Quantum Electron.*, **28**, 57 (1996).
20. Shilov A.A., Pasmanik G.A., Kulagin O.V. *Opt. Lett.*, **26**, 1565 (2001).
21. Zverev P.G., Basiev T.T., Osiko V.V., Kulkov A.M., Voitsekhovskii V.N., Yakobson V.E. *Opt. Mater.*, **11**, 315 (1999).
22. Foster J.D., Osterink L.M. *J. Appl. Phys.*, **41**, 3656 (1970).
23. Bonnefois A.M., Gilbert M., Thro P.-Y., Weulersse J.-M. *Opt. Commun.*, **259**, 223 (2006).
24. Siegman A.E. *Appl. Opt.*, **32**, 5893 (1993).